International Journal of Solids and Structures 49 (2012) 2349–2357

Contents lists available at SciVerse ScienceDirect

International Journal of Solids and Structures

journal homepage: www.elsevier.com/locate/ijsolstr

Mode-mixity-dependent adhesion of power-law graded elastic solids under normal load and substrate stretch-induced mismatch strain

Fan Jin, Xu Guo *

State Key Laboratory of Structural Analysis for Industrial Equipment, Department of Engineering Mechanics, Dalian University of Technology, Dalian 116023, China

ARTICLE INFO

Article history:
Received 12 November 2011
Received in revised form 4 May 2012
Available online 14 May 2012

Keywords:
Contact mechanics
Adhesion
Power-law graded materials
Mix mode
Mismatch strain

ABSTRACT

The present paper analytically investigates the adhesive behavior of power-law graded elastic solids under a combined action of external normal loading and a substrate stretch-induced mismatch strain with the effect of mode-mixity taken into account. A plane strain non-slipping model, a plane strain non-coupling model and an axisymmetric non-coupling model have been analyzed, respectively. Our results show that under a finite normal force, the equilibrium of the adhesive system may lost its stability at a critical value of mismatch strain, which significantly depends on both the graded material constants and the degree of mode-mixity. This indicates that the strongest or weakest adhesion strength under substrate stretching can be achieved by designing the physical constants of the adhesive system appropriately. These results provide a theoretical foundation for novel applications of functional graded materials in adhesion systems.

1. Introduction

The adhesive contact theories represented by JKR (Johnson et al., 1971), DMT (Derjaguin et al., 1975) and MD (Maugis, 1992) models have stimulated an explosion of theoretical development in the adhesion mechanics. These basic theories have been extended to a wider range including planar cases (Barquins, 1998; Chaudhury et al., 1996; Baney and Hui, 1997; Sundaram et al., 2012), various adhesive forces/potentials (Greenwood, 1997; Johnson and Greenwood, 1997; Barthel, 1998; Greenwood and Johnson, 1998), coupled normal and shear loads (Kim et al., 1998), periodic contact asperities (Johnson, 1995; Hui et al., 2001; Carbone and Mangialardi, 2004), rough surface contact (Fuller and Tabor, 1975; Persson, 2002; Guduru, 2007; Kesari and Lew, 2011) and viscoelastic materials (Greenwood and Johnson, 1981; Hui et al., 1998; Haiat et al., 2003). In recent years, the advancement in studies of adhesion is accelerated by growing interest in biology and biomimetics (Bhushan, 2009; Jagota and Hui, 2011). At the same time, various adhesion theories provide a powerful tool to reveal the physical mechanism behind the bio-adhesion phenomena. Various adhesion theories have been developed to understand adhesive behavior in bio-systems such as cell adhesion (Freund and Lin, 2004; Chu et al., 2005; Chen and Gao, 2006a,b,c, 2007b; Tsang et al., 2006; De et al., 2007; Walcott and Sun, 2010; Gao et al., 2011) and reversible adhesion systems of biological organisms (Artz et al., 2003; Glassmaker et al., 2004; Hui et al., 2004; Gao et al., 2005; Yao and Gao, 2006; Chen and Gao, 2007a; Autumn and Gravish, 2008; Chen et al., 2009; Pugno et al., 2011). It is worth noting that most of the above mentioned works are focused on the homogeneous materials.

On the other hand, the contact mechanics of functionally graded materials (FGMs) with controlled spatial variation of properties has become an important research topic for designing structures with exceptional resistance to deformation, fracture, fatigue and fiction induced damage (Suresh and Mortensen, 1998; Suresh, 2001). Many biological systems such as bones, teeth and conchiolin, have evolved the optimal surface properties for maximum functionality. For example, recent experimental observations show that the foam-like structure of cicada's pads consists of graded materials which exhibit robust flaw tolerant adhesion (Sherge and Gorb, 2001). It was also reported that some specific functionally graded hydroxyapatite coating can enhance the osteoblast adhesion significantly (Sandukas et al., 2011). Understanding the adhesive mechanism for FGMs can also provide us more possible approaches to achieve desired adhesion behavior by material design and optimization and hence may be helpful for solving many environmental and biological problems, such as biofouling induced by bacteria adhesion (Tsang et al., 2006). Thus, it is of great interest to study the adhesive behavior of materials with functionally graded elastic properties.

In contrast to the rapid progresses made in understanding the macro-scale Hertzian contact of elastic graded materials (Booker et al., 1985a,b; Popov, 1973b; Giannakopoulos and Suresh, 1997a,b; Giannakopoulos and Pallot, 2000), relatively little is known about the corresponding adhesive contact in micro-and

* Corresponding author. Tel.: +86 411 84707807.
E-mail address: guoxu@dlut.edu.cn (X. Guo).

0020-7683/$ - see front matter © 2012 Elsevier Ltd. All rights reserved.
http://dx.doi.org/10.1016/j.ijsolstr.2012.05.003

nano-scales. Yao and Gao (2010) found that a linearly graded elastic material (Gibson soil) can be designed to achieve flaw tolerant adhesion by employing an interfacial crack model. Meanwhile, the frictionless JKR model was successfully extended to power-law graded elastic solids in the plane strain case (Chen et al., 2009a) and the axisymmetric case (Chen et al., 2009b). Subsequently, the non-slipping JKR model was also established for power-law graded materials in the plane strain case (Jin and Guo, 2010) and in the axisymmetric case (Guo et al., 2011). The latter study revealed that the traditional frictionless model is exact for homogeneous incompressible solids as well as for linearly graded materials, and it is can be used as a good approximation for regular materials with positive Poisson's ratio even though the normal-tangential coupling effect is neglected. In fact, the exact non-slipping model is more preferable for auxetic materials with negative Poisson's ratio. In most of the above studies, an energy approach was used to establish the contact equilibrium conditions and the adhesion energy was assumed to be a material constant irrespective of the local fracture mode, which corresponds to the case of ideal elasticity with reversible adhesion.

However, the dissipative phenomena are common in most real processes involving interface interactions. For example, it was found that under both normal and tangential loadings (mixed-mode), the corresponding dissipative effect can increase the interface toughness significantly (Hutchinson and Suo, 1992). The same remains true in adhesive contact mechanics. Guduru and coworkers developed a phenomenological model to account for the effect of energy dissipation by assuming the effective work of adhesion is an increasing function of mode-mixity. With use of this model, they reexamined the contact problems in the presence of tangential loads or mismatch strains theoretically and experimentally (Waters and Guduru, 2010, 2011; Waters et al., 2012). More quantitatively accurate predictions of behavior were obtained after accounting for the mode-mixity dependence of work of adhesion. Chen et al. (2009) also introduced the effect of mode-mixity into their tape-substrate model to quantify the pre-tension-induced strongly reversible adhesion of the spatula pad. They found that the mode-mixity plays a key role in the adhesive response of an elastic thin pad adhering to a substrate.

On the other hand, recent studies revealed that stretching deformation can significantly influence the adhesion strength of contact systems. Chen and Gao (2006a,b,c, 2007b) established a series of adhesive contact models with substrate stretch-induced mismatch strain and showed that the pull-off force and the associated critical contact area tend to decrease with increasing substrate strain. Long and Hui (2012) found that the pre-stretch in membrane may reduce the energy release rate and increase the critical deflection for detachment. It is worth nothing that when substrate strain is taken into account, the failure mode of the adhesion system under normal loading will inevitably be mixed, and hence the dissipation phenomenon will come into play. Under this circumstance, the adhesive behavior of functionally graded elastic materials seems more complicated and hence remains elusive up to now.

The objective of the present study is to develop a fundamental understanding of the mode-mixity-dependent adhesive behavior of power-law graded elastic solids under substrate stretch-induced mismatch strain, which has not been addressed in previous research works. Following a general problem formulation in Section 2, a plane strain non-slipping model, a plane strain non-coupling model, and an axisymmetric non-coupling model have been analyzed in Section 3, respectively. All these models are established on the assumption that the work of adhesion is a function of mode-mixity. The effects of the material properties, the magnitude of mismatch strain and mode-mixity on adhesive behavior are also elucidated in this section. Finally, some concluding remarks are given in Section 4.

2. Problem formulation and solution procedures

Fig. 1 shows a rigid punch of radius R in adhesive contact with an elastically graded half-space under both a normal loading P (negative when tensile) and a substrate stretch-induced mismatch strain ε_m. In the plane strain case (2D), the punch is a cylinder and the stretch represents a uniaxial tension; while in the axisymmetric case (3D), the punch is a sphere and the stretch denotes an equibiaxial tension along the radius direction. The contact half-width (2D) or contact radius (3D) is measured by a. The graded half-space has a constant Poisson's ratio ν and a Young's modulus varied with depth according to a power-law form as

$$E = E_0(z/c_0)^k, \quad 0 < k < 1, \tag{2.1}$$

where E_0 is a reference modulus, $c_0 > 0$ a characteristic depth and k the gradient exponent. It is obvious that a homogeneous solid is recovered as $k = 0$.

2.1. Non-slipping plane strain contact

For the non-slipping plane strain contact case, the integral equation which relates the surface displacements of the half-space ($\bar{u}_x$ and $\bar{u}_z$) to the interfacial tractions within the contact region (σ_z and τ_{xz}) can be established with use of the surface Green's function as follows (Giannakopoulos and Pallot, 2000; Popov, 1973a):

$$\int_{-1}^{1} \frac{\operatorname{sign}(\xi-\eta) + \mathrm{i}\cot(\lambda\pi/2)}{|\xi-\eta|^k}\chi(\eta)\mathrm{d}\eta = g(\xi), \tag{2.2}$$

where

$$\begin{aligned} \chi(\xi) &= \kappa^{1/2}a^{1-k}\sigma_z(a\xi) + \mathrm{i}\kappa^{-1/2}a^{1-k}\tau_{xz}(a\xi), \\ g(\xi) &= \mathrm{i}\kappa^{-1/2}(\theta_1)^{-1}\bar{u}_z(a\xi) - \kappa^{1/2}(\theta_1)^{-1}\bar{u}_x(a\xi) \end{aligned} \tag{2.3}$$

with $\mathrm{i} = \sqrt{-1}$ and

$$\begin{aligned} &\lambda = \beta - 1, \quad \kappa = \frac{\beta}{1+k}, \quad \beta = \sqrt{(1+k)\left(1 - \frac{k\nu}{1-\nu}\right)}, \\ &\theta_1 = -\frac{c_0^k C_k \cos\frac{\beta\pi}{2}}{kE^*}, \quad E^* = \frac{E_0}{1-\nu^2}, \quad C_k = \frac{2^{1+k}\Gamma\left(\frac{3+k+\beta}{2}\right)\Gamma\left(\frac{3+k-\beta}{2}\right)}{\pi\Gamma(2+k)}, \end{aligned} \tag{2.4}$$

where $\Gamma(\cdot)$ denotes the Gamma function. According to Popov (1973a), the exact solution of the integral equation in (2.2) can be expressed as

$$\chi(\xi) = \sum_{m=0}^{\infty} \frac{g_m P_m^{\rho}(\xi)}{\mathrm{i}\varrho\lambda_m\psi_{\rho}^{2\mathrm{D}}(\xi)}, \tag{2.5}$$

where $P_m^{\rho}(\xi) = P_m^{-w-\mathrm{i}\rho,-w+\mathrm{i}\rho}(\xi)$ is the Jacobi polynomial of order m with index $(-w-\mathrm{i}\rho, -w+\mathrm{i}\rho)$ and

$$\begin{aligned} &\psi_{\rho}^{2\mathrm{D}}(\xi) = (1-\xi)^{w+\mathrm{i}\rho}(1+\xi)^{w-\mathrm{i}\rho}, \quad \rho = \frac{1}{2\pi}\ln\frac{\sin[(k+\lambda)\pi/2]}{\sin[(k-\lambda)\pi/2]}, \\ &w = \frac{1-k}{2}, \quad \varrho = \frac{2\pi\sqrt{\sin[(k+\lambda)\pi/2]\sin[(k-\lambda)\pi/2]}}{\sin(k\pi)\sin(\lambda\pi/2)}, \\ &g_m = \int_{-1}^{1}\frac{g(\xi)P_m^{-\rho}(\xi)}{\psi_{-\rho}^{2\mathrm{D}}(\xi)}\mathrm{d}\xi, \quad \lambda_m = \frac{2^k|\Gamma(1-w+\mathrm{i}\rho+m)|^2}{m!^2(k+2m)\Gamma(k)}. \end{aligned} \tag{2.6}$$

Additionally, the force applied on the cylindrical punch can be expressed as

$$P = \frac{g_0 a^k}{\mathrm{i}\kappa^{1/2}\varrho}. \tag{2.7}$$

For prescribed surface displacements of the substrate ($\bar{u}_x$ and $\bar{u}_z$), χ can be determined from Eq. $(2.3)_2$, $(2.6)_5$, (2.7) and (2.5), hence the interfacial tractions (σ_z and τ_{xz}) can be further obtained from its real and imaginary parts according Eq. $(2.3)_1$, respectively.

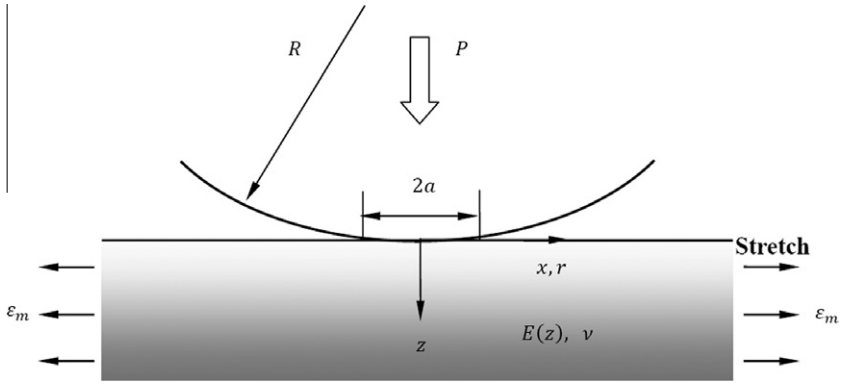

Fig. 1. Schematic of a rigid punch (cylinder for 2D; sphere for 3D) in adhesive contact with a power-law graded half-space under a normal loading P (negative when tensile) and a stretch-induced mismatch strain ε_m.

2.2. Non-slipping axisymmetric contact

For the non-slipping axisymmetric contact case, as pointed out by Popov (1973b), the interfacial tractions (σ_z and τ_{rz}) within the contact region can be obtained from the surface displacements of the half-space ($\bar{u}_r$ and $\bar{u}_z$) as

$$\sigma_z(r) = -\kappa^{-\frac{1}{2}}\frac{\mathrm{d}}{\mathrm{d}r}\int_r^a \frac{s\mathrm{Re}[\hat{\chi}(s)]}{r\sqrt{s^2-r^2}}\mathrm{d}s,$$
$$\tau_{rz}(r) = -\kappa^{\frac{1}{2}}\frac{\mathrm{d}}{\mathrm{d}r}\int_r^a \frac{\mathrm{Im}[\hat{\chi}(s)]}{\sqrt{s^2-r^2}}\mathrm{d}s, \tag{2.8}$$

where $\mathrm{Re}[\hat{\chi}(s)]$ and $\mathrm{Im}[\hat{\chi}(s)]$ denote the real and imaginary parts of $\hat{\chi}(s)$, respectively.

In Eq. (2.8),

$$\hat{\chi}(x) = \sum_{m=0}^{\infty}\frac{\hat{\chi}_m P_m^{\rho}(x)}{\psi_{\rho}^{3\mathrm{D}}(x)}, \quad \psi_{\rho}^{3\mathrm{D}}(x) = (a-x)^{-\frac{k}{2}+\mathrm{i}\rho}(a+x)^{-\frac{k}{2}-\mathrm{i}\rho},$$
$$\hat{\chi}_m = \frac{(m!)^2(1+k+2m)\Gamma(k)\sin(k\pi/2)\cosh(\pi\rho)}{\pi(2a)^{1+k}|\Gamma(1+m+k/2+\mathrm{i}\rho)|^2}H_m,$$
$$H_m = \int_{-a}^{a}\frac{H'(x)P_m^{-\rho}(x)}{\psi_{-\rho}^{3\mathrm{D}}(x)}\mathrm{d}x, \quad m = 0,1,2,\ldots \tag{2.9}$$
$$H(x) = \frac{2x\tan(\lambda\pi/2)}{\pi\theta_1\sqrt{\kappa}\tan(k\pi/2)}\int_0^1 \frac{[\bar{u}_z(xt)t + \mathrm{i}\kappa\bar{u}_r(xt)]}{\sqrt{1-t^2}}\mathrm{d}t$$

with $H'(x) = \mathrm{d}H/\mathrm{d}x$.

In addition, the force applied on the spherical punch can be written as

$$P = \frac{\sin(k\pi/2)\cosh(\pi\rho)}{k\sqrt{\kappa}}\mathrm{Re}[H_0]. \tag{2.10}$$

In the above non-slipping contact models, coupling effect exists between the normal and tangential deformations, which leads to the oscillatory singularity of the interfacial stresses near the contact edge. As demonstrated by Guo et al. (2011), the magnitude of the coupling effect is controlled by a material parameter, ρ defined in Eq. $(2.6)_2$, which vanishes for homogeneous incompressible as well as for linearly graded materials, and becomes relatively small for regular materials with positive Poisson's ratios. Under this circumstance, the non-coupling contact model with non-oscillatory interfacial tractions (i.e., 'frictionless model' in the absence of mismatch strain) can be adopted as a good approximation (Chen et al., 2009b). In the following, the effect of mode-mixity under both the normal load and the mismatch strain will be discussed in details for different adhesive contact models, respectively.

3. Analysis results

3.1. Plane strain non-slipping adhesion

Under a mismatch strain ε_m and the parabolic assumption of local contact surfaces, the displacements across the contact interface can be expressed as

$$\bar{u}_x = \varepsilon_m x, \quad \bar{u}_z = h - \frac{x^2}{2R}, \quad |x| \leqslant a, \tag{3.1}$$

where R is the radius of the rigid cylinder and h denotes the depth of indentation. Combining Eqs. (3.1), $(2.3)_2$, $(2.6)_5$, (2.7) and (2.5) gives rise to an oscillatory stress field as

$$\sigma_z(x) = \frac{1}{(a^2-x^2)^{\frac{1-k}{2}}}\left\{I_1\cos\left(\rho\ln\frac{a+x}{a-x}\right) - I_2\sin\left(\rho\ln\frac{a+x}{a-x}\right)\right\},$$
$$\tau_{xz}(x) = \frac{\kappa}{(a^2-x^2)^{\frac{1-k}{2}}}\left\{I_2\cos\left(\rho\ln\frac{a+x}{a-x}\right) + I_1\sin\left(\rho\ln\frac{a+x}{a-x}\right)\right\}, \tag{3.2}$$

where

$$I_1 = \frac{\Gamma(1+k)}{(2a)^k\varpi}P + \frac{1}{\kappa\theta_1 R}\frac{(1+4\rho^2)a^2-(2+k)x^2}{(2+k)(1+k)k\varrho} + \frac{2\rho a\varepsilon_m}{\theta_1 k(1+k)\varrho},$$
$$I_2 = \frac{x}{\theta_1(1+k)k\varrho}\left[\frac{2\rho a}{\kappa R} + (1+k)\varepsilon_m\right], \tag{3.3}$$

and

$$\varpi = \Gamma\left(\frac{1+k}{2}+\mathrm{i}\rho\right)\Gamma\left(\frac{1+k}{2}-\mathrm{i}\rho\right). \tag{3.4}$$

The quantity ρ defined in Eq. $(2.6)_2$ is the so-called normal-tangential coupling parameter, which leads to an oscillatory stress field. Since ρ becomes zero for homogeneous incompressible and linearly graded materials, the corresponding non-coupling model provides exact solutions (Guo et al., 2011).

For this plane strain non-slipping model, the corresponding complex-valued stress intensity factor and the energy release rate were introduced by Guo et al. (2011) in the absence of mismatch strain. As the substrate stretch induced- mismatch strain is involved, they are derived as (see Appendix A for details)

$$K = K_{\mathrm{I}} + \mathrm{i}K_{\mathrm{II}} = \sqrt{2\pi}\ \lim_{x\to a}(a-x)^{\frac{1-k}{2}+\mathrm{i}\rho}\left(\sigma_z + \frac{\mathrm{i}}{\kappa}\tau_{xz}\right) \tag{3.5}$$

and

$$G = \frac{1}{2}\frac{\kappa\theta_1 k\varrho\varpi}{2\pi\Gamma(1+k)}|K|^2, \tag{3.6}$$

respectively.

The $P-a-\varepsilon_m$ relation of the considered contact system can be obtained by setting the energy release rate equal to the effective work of adhesion ω_{ad}, which depends on the phase angle of mode-mixity ψ defined in the form of

$$\psi=\tan^{-1}\frac{Im[Kl^{-i\rho}]}{Re[Kl^{-i\rho}]}. \tag{3.7}$$

In Eq. (3.7), l denotes a reference length. Different expressions of mode-mixity-dependent adhesion energy (interfacial fracture toughness) can be found in Hutchinson and Suo (1992). One of them, which is adopted in the present study, has the following expression

$$\omega_{ad}(\psi)=\Delta\gamma\xi(\psi)=\frac{\Delta\gamma}{1-(1-\lambda_0)\sin^2\psi},\quad 0\leqslant\lambda_0\leqslant 1 \tag{3.8}$$

where $\Delta\gamma$ is the work of adhesion under pure mode I loading condition and the parameter λ_0 determines the influence of mode-mixity. Fig. 2 plots the variation $\omega_{ad}/\Delta\gamma$ with respect to ψ for different values of λ_0. Especially, when $\lambda_0=1$, it yields that $\omega_{ad}=\Delta\gamma$, which coincides with the classical surface energy.

With use of Eqs. (3.2), (3.5) and (3.6), the $P-a-\varepsilon_m$ relation can be established from $G=\omega_{ad}(\psi)$ as

$$\left[\frac{\Gamma(1+k)\widehat{P}}{2^k\varpi\hat{a}^k}-\frac{1}{2\pi\kappa d_1 k\varrho}\frac{(1+k-4\rho^2)\alpha^k\hat{a}^2}{(2+k)(1+k)\widehat{R}^k}+\frac{\rho\alpha^k\hat{a}\widehat{R}^{1-k}\varepsilon_m}{\pi d_1 k\varrho(1+k)}\right]^2+\left\{\frac{\alpha^k\hat{a}\widehat{R}^{1-k}}{2\pi d_1 k\varrho}\left[\frac{2\rho\hat{a}}{(1+k)\kappa\widehat{R}}+\varepsilon_m\right]\right\}^2-\frac{\Gamma(1+k)\alpha^k\hat{a}^{1-k}\xi(\psi)}{2^{5+k}\pi\kappa d_1 k\sigma_k\varpi\widehat{R}^k}=0, \tag{3.9}$$

where

$$\hat{a}=\frac{a}{a_{2D0}},\quad \widehat{R}=\frac{R}{a_{2D0}},\quad \widehat{P}=\frac{PR}{2\pi E^* a_{2D0}^2}$$
$$\alpha=\frac{R}{c_0},\quad d_1=-\frac{C_k\cos\frac{\beta\pi}{2}}{k} \tag{3.10}$$

are all dimensionless quantities. The quantity $a_{2D0}=\sqrt[3]{32R^2\Delta\gamma/(\pi E^*)}$ in Eq. (3.10) is the classical 2D-JKR contact half-width corresponding to $\varepsilon_m=0$ and $P=0$, which can also be obtained from Eq. (3.9) by setting $k=0$, $\rho=0$, $\varepsilon_m=0$ and $\lambda_0=1$ simultaneously.

Fig. 3a-b show the normalized contact half-width a/a_{2D0} as a function of the mismatch strain ε_m for a specific graded half-space ($k=0.5$) under different loading cases. In the absence of applied force ($\widehat{P}=0$), as shown in Fig. 3a, $\hat{a}$ decreases smoothly to zero with increasing ε_m. Thus it is not easy to break up the adhering system by stretch alone. However, the presence of a finite pulling force ($\widehat{P}<0$) can lead to a quite different result. As shown in Fig. 3b, there always exists a critical mismatch strain ε_{cr} beyond which the adhesion system will lost its stability and hence the punch is predicted to break apart from the substrate spontaneously. The same phenomenon were also observed for homogeneous materials even though the normal-tangential coupling are neglected (Chen and Gao, 2007b; Waters et al., 2012).

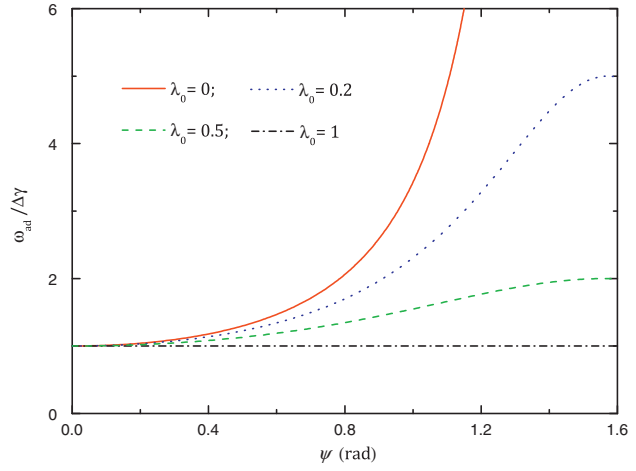

Fig. 2. Variation of the work of adhesion with respect to the phase angle of mode-mixity ψ, for different values of λ_0.

3.2. Plane strain non-coupling adhesion

In this contact model, the normal-tangential coupling effect has been neglected. The corresponding non-oscillatory interfacial stress distributions within the contact region can be obtained by letting $\rho=0$ in Eq. (3.2) as

$$\sigma_z(x)=d_2(a^2-x^2)^{\frac{k-1}{2}}+\frac{E^*}{\pi R}\frac{\cos\frac{k\pi}{2}}{c_0^k C_k\beta\sin\frac{\beta\pi}{2}}(a^2-x^2)^{\frac{k+1}{2}},$$
$$\tau_{xz}(x)=\frac{\kappa E^*\cos\frac{k\pi}{2}}{\pi c_0^k C_k\ \sin\frac{\beta\pi}{2}}\frac{x\varepsilon_m}{(a^2-x^2)^{\frac{1-k}{2}}}, \tag{3.11}$$

where

$$d_2=\frac{\Gamma(1+k)}{(2a)^k\left[\Gamma\left(\frac{1+k}{2}\right)\right]^2}P-\frac{(1+k)\cos\frac{k\pi}{2}}{(2+k)c_0^k C_k\beta\ \sin\frac{\beta\pi}{2}}\frac{E^*a^2}{\pi R}. \tag{3.12}$$

Consequently, the stress intensity factors K_I and K_{II} are defined as

$$K_I=\sqrt{2\pi}\lim_{x\to a^-}(a-x)^{\frac{1-k}{2}}\sigma_z(x),$$
$$K_{II}=\frac{\sqrt{2\pi}}{\kappa}\lim_{x\to a^-}(a-x)^{\frac{1-k}{2}}\tau_{xz}(x). \tag{3.13}$$

With use of K_I and K_{II}, the corresponding energy release rate can be calculated from Eq. (3.6) as

$$G=\frac{K_I^2+K_{II}^2}{2M}, \tag{3.14}$$

where

$$M=d_3\frac{E^*}{c_0^k},\quad d_3=\frac{2^{1+k}(1+k)\cos\frac{k\pi}{2}}{\sqrt{\pi}C_k\beta\sin\frac{\beta\pi}{2}}\frac{\Gamma\left(1+\frac{k}{2}\right)}{\Gamma\left(\frac{1+k}{2}\right)}. \tag{3.15}$$

Letting $G=\omega_{ad}(\psi)$, the $P-a-\varepsilon_m$ relation can be found as

$$\left[\frac{\Gamma(1+k)d_5C_k\cos\frac{\beta\pi}{2}}{2^k d_4\hat{a}^k}\widehat{P}+\frac{1}{2\pi\kappa}\frac{\alpha^k\hat{a}^2}{(2+k)\widehat{R}^k}\right]^2+\left[\frac{\alpha^k\hat{a}\widehat{R}^{1-k}}{2\pi}\varepsilon_m\right]^2+\frac{\Gamma(1+k)d_5C_k\cos\frac{\beta\pi}{2}\alpha^k\hat{a}^{1-k}\xi(\psi)}{2^{5+k}\pi\kappa d_4\widehat{R}^k}=0, \tag{3.16}$$

where

$$d_4=\Gamma^2\left(\frac{1+k}{2}\right),\quad d_5=-\frac{\pi\tan(\beta\pi/2)}{\cos(k\pi/2)} \tag{3.17}$$

and

$$\psi=\tan^{-1}(K_{II}/K_I). \tag{3.18}$$

Fig. 4a-b depict the normalized contact half-width a/a_{2D0} versus the mismatch strain ε_m for various values of mode-mixity parameter λ_0 under zero and finite normal loading, respectively. In homogeneous case, a/a_{2D0} depends on ε_m and $\widehat{R}$ only through the combined parameter $\widehat{R}\varepsilon_m$ (Chen and Gao, 2007b). For power-law law graded materials ($k\neq 0$), however, $\widehat{R}$ and ε_m affect the behavior of a/a_{2D0} independently. As can be seen from Fig. 4a-b, for a specific

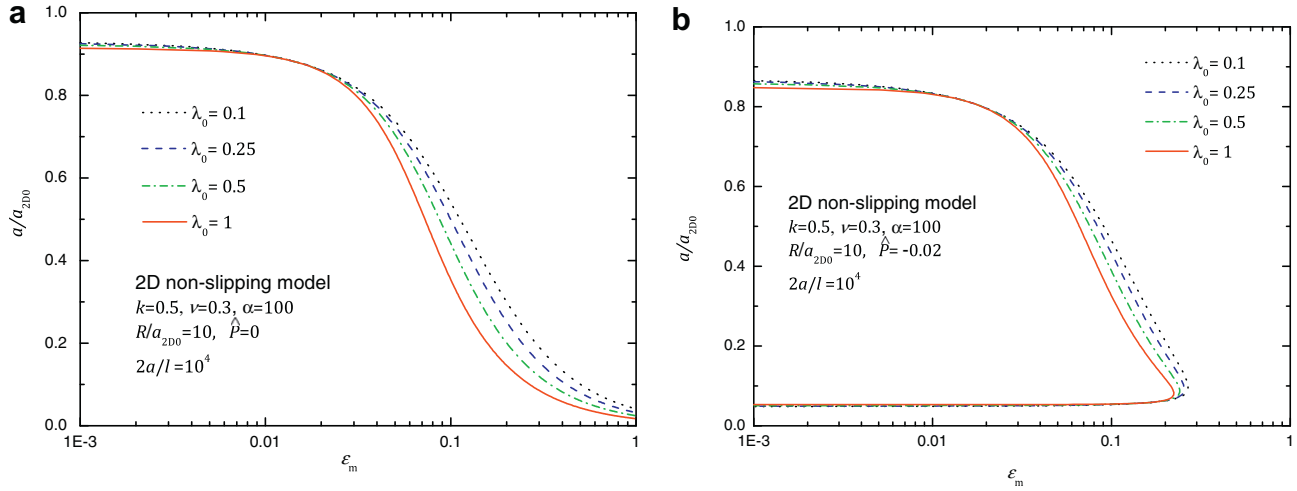

Fig. 3. Variation of the normalized contact half-width a/a_{2D0} as a function of the mismatch strain ε_m in the plane strain non-slipping model with respect to the gradient exponent $k = 0.5$ under (a) zero and (b) finite normal loading.

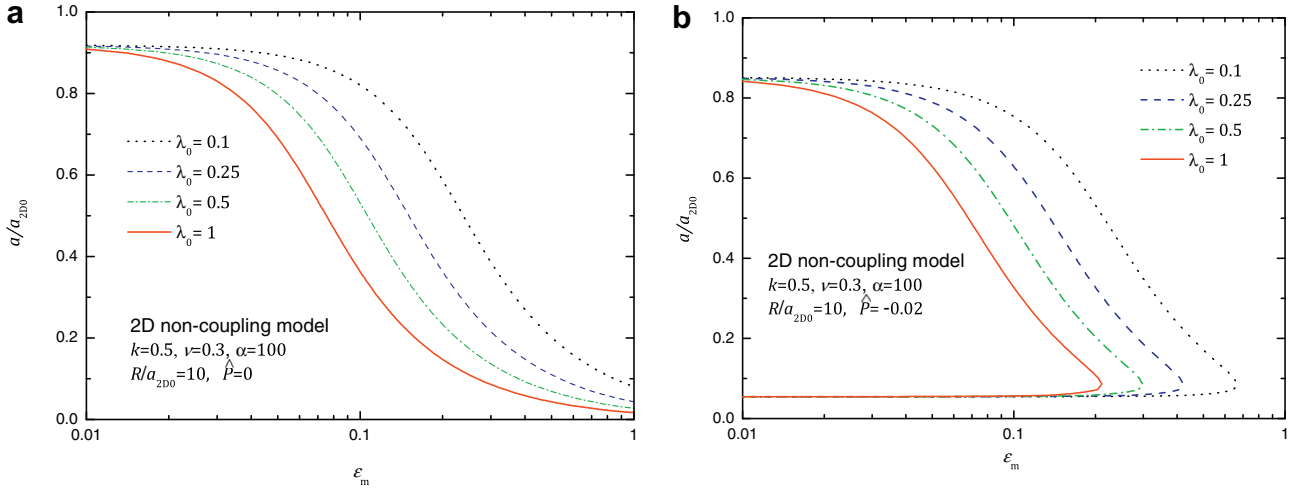

Fig. 4. Variation of the normalized contact half-width a/a_{2D0} as a function of the mismatch strain ε_m in the plane strain non-coupling model with respect to the gradient exponent $k = 0.5$ under (a) zero and (b) finite normal loading.

value of ε_m, the smaller the value of λ_0, the larger the value of a/a_{2D0}. This is due to decreasing the mode-mixity will enhance the energy dissipation on the interface and further make the adhesive contact system more stable. The reversible adhesion ($\lambda_0 = 1$) may underpredict the contact half-width for a given value of ε_m.

To investigate behavior of the critical mismatch strain under a finite normal force, Fig. 5a-c plot the variation of ε_{cr} with respect to the gradient exponent k for various values of $\widehat{R}$, α, λ_0, and $\widehat{P}$ (negative when tensile), respectively. As shown in Fig. 5a, ε_{cr} increases monotonically with k when α is relatively large while for small α, ε_{cr} will attain a maximum value at some specific values of k (<1). Just as seen from Fig. 5b-c, there always exist a maximum ε_{cr} at some specific value of k(<1) for the given parameters. Under this circumstance, it is possible to achieve the strongest adhesion strength (maximum ε_{cr}) by selecting the material constants (α, k and $\widehat{R}$) appropriately.

3.3. Axisymmetric non-coupling adhesion

In this axisymmetric contact model, the punch is a rigid sphere of radius R, and its profile is approximated as a parabola, i.e., $f(r) = r^2/2R$, Under this assumption, the oscillatory interfacial stress field within the contact region has been derived by Guo et al. (2011). Again, by letting $\rho = 0$, the corresponding non-oscillatory interfacial stress field within the contact region can be recovered as

$$\begin{aligned}\sigma_z(r) &= C_1\left[1-\left(\frac{r}{a}\right)^2\right]^{\frac{1+k}{2}} + C_2\left[1-\left(\frac{r}{a}\right)^2\right]^{\frac{k-1}{2}},\\ \tau_{rz}(r) &= \frac{2\kappa\cos\frac{k\pi}{2}}{\pi^{3/2}C_k\sin\frac{\beta\pi}{2}}\frac{\Gamma\left(1+\frac{k}{2}\right)}{\Gamma\left(\frac{3+k}{2}\right)}\frac{E^*}{c_0^k}r(a^2-r^2)^{\frac{k-1}{2}}\varepsilon_m,\end{aligned} \tag{3.19}$$

where

$$\begin{aligned}C_1 &= \frac{4a^{1+k}E^*\cos(k\pi/2)}{\pi^{3/2}Rc_0^kC_k\beta\sin(\beta\pi/2)}\frac{\Gamma(1+k/2)}{(1+k)\Gamma(1/2+k/2)},\\ C_2 &= \frac{P(1+k)}{2\pi a^2} - \frac{4a^{1+k}E^*\cos(k\pi/2)}{\pi^{3/2}Rc_0^kC_k\beta\sin(\beta\pi/2)}\frac{\Gamma(1+k/2)}{(3+k)\Gamma(1/2+k/2)}\end{aligned} \tag{3.20}$$

and the material constants κ,β and C_k are defined in Eq. (2.4). The stress field for homogeneous material (Chen and Gao, 2009b) can

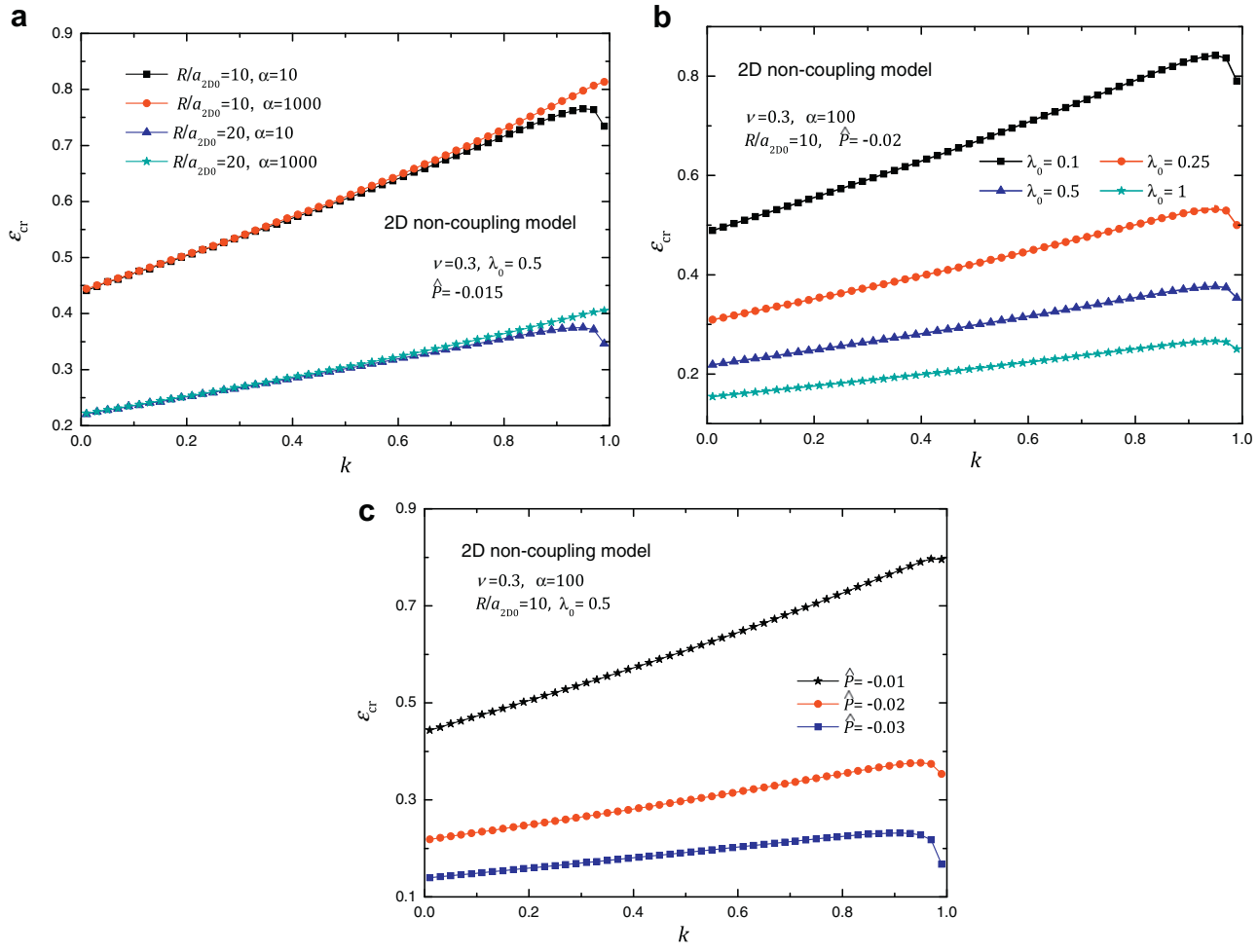

Fig. 5. Variation of the critical mismatch strain ε_{cr} with respect to the gradient exponent k in the plane strain non-coupling model for various values of (a) material constants $\widehat{R}$ and α, (b) mode-mixity parameter λ_0, as well as (c) normal loading $\widehat{P}$.

be recovered in the limit of $k \to 0$ in Eq. (3.19). Similar to that in the plane strain non-coupling model, the stress intensity factors K_I and K_{II} are defined as

$$K_I = \sqrt{2\pi}\lim_{r\to a^-}(a-r)^{\frac{1-k}{2}}\sigma_z(r),$$
$$K_{II} = \frac{\sqrt{2\pi}}{\kappa}\lim_{r\to a^-}(a-r)^{\frac{1-k}{2}}\tau_{rz}(r) \tag{3.21}$$

and the corresponding energy release rate can be written as

$$G = \frac{K_I^2 + K_{II}^2}{2M}, \tag{3.22}$$

where

$$M = d_3\frac{E^*}{c_0^k}, \quad d_3 = \frac{2^{1+k}(1+k)\cos\frac{k\pi}{2}}{\sqrt{\pi}C_k\beta\sin\frac{\beta\pi}{2}}\frac{\Gamma(1+k/2)}{\Gamma\left(\frac{1+k}{2}\right)}. \tag{3.23}$$

Combining Eqs. (3.19)–(3.23) and equating G to the effective work of adhesion, $\omega_{ad}(\psi)$, expressed in Eq. (3.8), the $P-a-\varepsilon_m$ relation can be expressed as

$$\frac{9C_3\alpha^k}{2\widehat{R}^k}\hat{a}^{3+k} - 6C_4\widehat{P} + \frac{8C_5\widehat{R}^k}{\alpha^k}\frac{\widehat{P}^2}{\hat{a}^{3+k}} + \frac{9C_6}{2}\alpha^k\widehat{R}^{2-k}\hat{a}^{1+k}\varepsilon_m^2 - \xi(\psi) = 0, \tag{3.24}$$

where

$$C_3 = \frac{2^{2+k}}{\beta(3+k)}C_7C_8, \quad C_4 = \frac{1}{3+k} \quad C_5 = \frac{\beta\Gamma(2+k)}{2^{4+k}C_7},$$
$$C_6 = \frac{2^{2+k}(3+k)\kappa}{1+k}C_7C_8, \quad C_7 = \frac{\left[\Gamma\left(1+\frac{k}{2}\right)\right]^2\cos\frac{k\pi}{2}}{\pi C_k\ \sin(\beta\pi/2)}, \quad C_8 = \frac{2+k}{\Gamma(4+k)},$$
$$\hat{a} = \frac{a}{a_{3D0}}, \quad \widehat{R} = \frac{R}{a_{3D0}}, \quad \widehat{P} = \frac{3PR}{4E^*a_{3D0}^3}, \quad \alpha = \frac{R}{c_0} \tag{3.25}$$

are all dimensionless quantities, ψ is the mode-mixity angle defined in Eq. (3.18) and $a_{3D0} = \sqrt[3]{9\pi R^2\Delta\gamma/(2E^*)}$ is the classical JKR contact radius corresponding to $\varepsilon_m = 0$ and $P = 0$ simultaneously. Note that $\hat{a}, \widehat{R}$, and $\widehat{P}$ defined in Eq. (3.25) are different from that given in Eq. (3.10) for 2D case. From Eq. (3.22), it can be predicted that pull-off force can be reduced due to the presence of the mismatch strain. This can be interpreted from an energy point view such that since extra elastic energy induced by substrate strain is stored at the interface, then it needs less work for normal load to initiate the detachment of the contact system. This result may be of interest for the designing of thin or multilayered coating systems where the presence of residual stresses may reduce its adhesive performance.

Fig. 6a-b depict the normalized contact radius a/a_{3D0} versus the mismatch strain ε_m for various values of mode-mixity parameter λ_0 under zero and finite normal loading, respectively. Qualitatively similar to that in the 2D model, the behavior of a/a_{3D0} is expected to exhibit two different variation trends depending on the value of

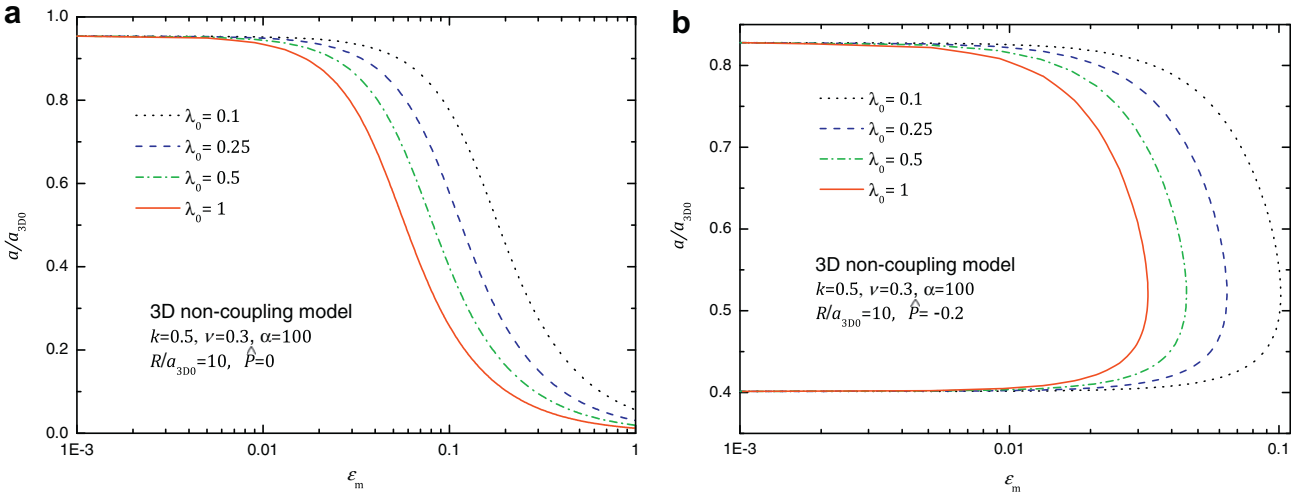

Fig. 6. Variation of the normalized contact radius a/a_{3D0} as a function of the mismatch strain ε_m in the axisymmetric non-coupling model with respect to the gradient exponent $k = 0.5$ under (a) zero and (b) finite normal loading.

P. Detailed discussions can be found in the previous two subsections.

Fig. 7a-c plot the variation of ε_{cr} with respect to the gradient exponent k for various values of $\hat{R}$, α,λ_0, and $\hat{P}$ (negative when tensile). As observed from Fig. 7a, the behavior of ε_{cr} is quite different for different values of α. For example, when $\alpha = 100$, ε_{cr} is a monotonically increasing function of k; while for $\alpha = 10^4$, ε_{cr} will attain a minimum value at some specific value of k. Different from that in Fig. 5b-c (2D), the adhesion in Fig. 7b-c shows that weakest strength can be achieved by selecting the material constants

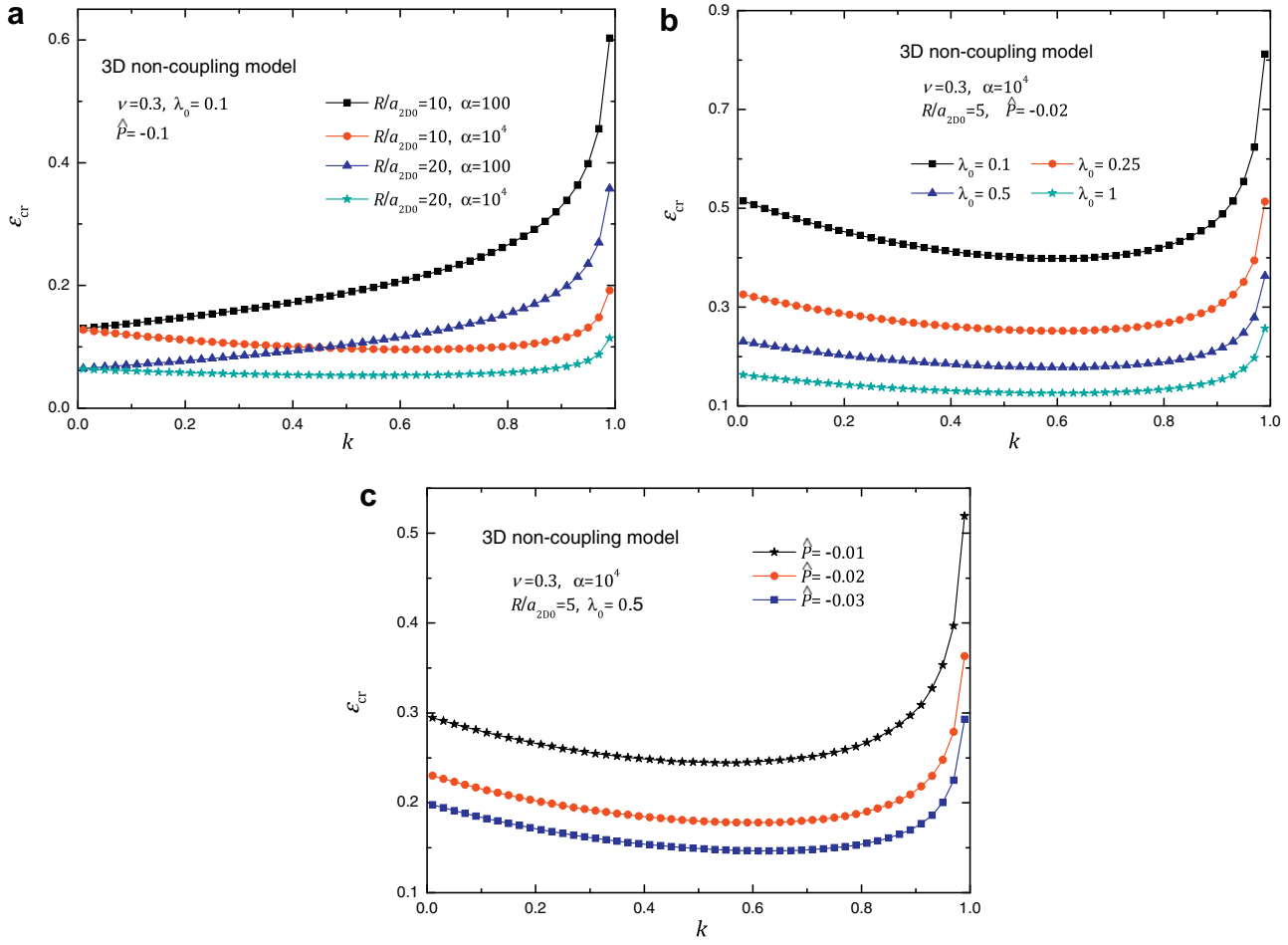

Fig. 7. Variation of the critical mismatch strain ε_{cr} with respect to the gradient exponent k in the axisymmetric non-coupling model for various values of (a) material constants $\hat{R}$ and α, (b) mode-mixity paramer λ_0, as well as (c) normal loading $\hat{P}$.

appropriately. In addition, it can also be observed that the critical mismatch strain ε_{cr} is predicted to be reduced by increasing the magnitudes of λ_0 and $\widehat{P}$, that is, both increasing energy dissipation and decreasing pulling force can substantially stabilize the adhesive system.

4. Conclusions

In traditional adhesive contact models, the work of adhesion is often assumed to be independent of the mode-mixity, which may underestimate the energy dissipation under some circumstances. Although some results about the effect of mode-mixity have been reported for homogeneous materials, the effect of mode mixity remains elusive for graded elastic materials especially when the substrate stretching-induced mismatch strain is involved. The present study has analytically examined the effects of mode-mixity and mismatch strain on adhesive behavior for three different contact models in details. It has been found that the material constants of graded materials have significant influence on the contact behavior of adhesive systems especially in the presence of substrate strain. The results obtained here can provide useful insights on the design of adhesion systems with use of graded materials.

Acknowledgements

The financial supports from the National Natural Science Foundation (10932003 and 10925209), 973 Project of China (2010CB832703), Program for Changjiang Scholars and Innovative Research Team in University (PCSIRT) and the Fundamental Research Funds for the Central Universities (DUT11ZD104) are gratefully acknowledged.

Appendix A. Stress intensity factor and energy release rate

Based on the interfacial tractions described in Eq. (3.2), a complex-valued stress intensity factor is introduced as

$$K = \sqrt{2\pi}\ \lim_{x\to a}(a-x)^{\frac{1-k}{2}+i\rho}(\sigma_z + i\tau_{xz}/\kappa) = \sqrt{2\pi}(2a)^{\frac{k-1}{2}+i\rho}(I_{10}+iI_{20}), \tag{A1}$$

where

$$I_{10} = \frac{\Gamma(1+k)}{(2a)^k R_k}P - \frac{1}{\kappa\theta_1 R}\frac{(1+k-4\rho^2)a^2}{(2+k)(1+k)k\varrho} + \frac{2\rho a\varepsilon_m}{\theta_1 k(1+k)\varrho},$$
$$I_{20} = \frac{a}{\theta_1(1+k)k\varrho}\left[\frac{2\rho a}{\kappa R} + (1+k)\varepsilon_m\right]. \tag{A2}$$

The combined interfacial traction at a distance η ahead the rim of the contact region can be rewritten as

$$\left(\sigma_z + \frac{i}{\kappa}\tau_{xz}\right)\Big|_{x=a-\eta} = \frac{K}{\sqrt{2\pi}}\eta^{\frac{k-1}{2}-i\rho}. \tag{A3}$$

While the complex discontinuity of the displacement (opening/sliding gap) can be calculated as (Maugis, 1992)

$$[\bar{u}_z] + i\kappa[\bar{u}_x] = (\bar{u}_z + i\kappa\bar{u}_x) + \frac{x^2}{2R} - h - i\kappa\varepsilon_m x, \quad |x| > a, \tag{A4}$$

where the depth of penetration h can be derived as

$$h = \frac{\theta_1\varrho\kappa\Gamma(1+k)}{(2a)^k\varpi}P + \frac{a^2}{2R}\frac{1+k-4\rho^2}{(1+k)(2+k)} - \frac{2\rho\kappa a\varepsilon_m}{1+k}. \tag{A5}$$

Outside the contact region $x = a + \eta$, the complex surface displacement of the substrate is

$$\bar{u}_z + i\kappa\bar{u}_x = -\kappa\theta_1\left(\tan\frac{\beta\pi}{2} + i\right)\int_{-a}^{a}\frac{\sigma_z(s) + i\tau_{xz}(s)/\kappa}{(a+\eta-s)^k}ds. \tag{A6}$$

Substituting Eqs. (3.2) and (3.3) into Eq. (A6) and using the fact that as $\eta \to 0^+$

$$\int_{-a}^{a}\frac{s^n(a+s)^{\frac{k-1}{2}+i\rho}(a-s)^{\frac{k-1}{2}-i\rho}}{(a+\eta-s)^k}ds \to \frac{D_n}{\cos[\pi(k/2+i\rho)]} - \frac{2k\varpi a^n}{(1-k-2i\rho)\Gamma(1+k)}\left(\frac{\eta}{2a}\right)^{\frac{1-k}{2}-i\rho}, \quad n = 0,1,2 \tag{A7}$$

where

$$D_0 = \pi, \quad D_1 = \pi a(k+2i\rho),$$
$$D_2 = \pi a^2(1+k^2-4\rho^2+4ik\rho). \tag{A8}$$

The asymptotic discontinuity of the displacement along the interface ahead of the contact edge behaves as

$$([\bar{u}_z] + i\kappa[\bar{u}_x])|_{x=a+\eta} = \frac{2\kappa\theta_1[\tan(\beta\pi/2)+i]k\varpi}{(1-k-2i\rho)\Gamma(1+k)}\frac{K}{\sqrt{2\pi}}\eta^{\frac{1-k}{2}-i\rho}, \tag{A9}$$

where the identity

$$\sigma_k = -\frac{\pi[\tan(\beta\pi/2)+i]}{\cos[\pi(k/2+i\rho)]} \tag{A10}$$

has been used.

The elastic energy dU associated with the contact size increasing da at the contact edge can be calculated as

$$dU = \frac{1}{2}\int_0^{da}\overline{[\sigma_z + i\tau_{xz}/\kappa]}\{[u_z] + i\kappa[u_x]\}d\eta = \frac{\kappa\theta_1[\tan(\beta\pi/2)+i]k\varpi}{(1-k-2i\rho)\Gamma(1+k)}\frac{|K|^2}{2\pi}\int_0^{da}\left(\frac{\eta}{da-\eta}\right)^{\frac{k-1}{2}+i\rho}d\eta = -\frac{\kappa\theta_1 k\varrho\varpi}{4\pi\Gamma(1+k)}|K|^2 da, \tag{A11}$$

where the formula

$$\int_0^{da}\eta^{\frac{k-1}{2}+i\rho}(da-\eta)^{\frac{1-k}{2}-i\rho}d\eta = \frac{\pi[(1-k)-2i\rho]}{2\cos[\pi(k/2+i\rho)]}da \tag{A12}$$

has been employed. Consequently, the energy release rate is

$$G = -\frac{dU}{da} = \frac{1}{2}\frac{\kappa\theta_1 k\varrho\varpi}{2\pi\Gamma(1+k)}|K|^2, \tag{A13}$$

which is a generalized version of the classical energy release rate for homogeneous materials (Rice, 1988).

References

Artz, E., Gorb, S., Spolenak, R., 2003. From micro to nano contacts in biological attachment devices. Proc. Natl. Acad. Sci. USA 100, 10603–10606.
Autumn, K., Gravish, N., 2008. Gecko adhesion: evolutionary nanotechnology. Phil. Trans. R. Soc. A 366, 1575–1590.
Baney, J.M., Hui, C.Y., 1997. A cohesive zone model for the adhesion of cylinders. J. Adhesion Sci. Technol. 11, 393–406.
Barquins, M., 1998. Adherence and rolling kinetics of a rigid cylinder in contact with a natural rubber surface. J. Adhesion 26, 1–12.
Barthel, E., 1998. On the description of the adhesive contact of spheres with arbitrary interaction potentials. J. Coll. Interface Sci. 200, 7–18.
Bhushan, B., 2009. Biomimetics: lessons from nature-an overview. Phil. Trans. R. Soc. A 367, 1445–1486.
Booker, J.R., Balaam, N.P., Davis, E.H., 1985a. The behavior of an elastic non-homogeneous half-space. Part I. Line and point loads. Int. J. Numer. Anal. Methods Geomech. 9, 353–367.
Booker, J.R., Balaam, N.P., Davis, E.H., 1985b. The behavior of an elastic non-homogeneous half-space. Part II. Circular and strip footings. Int. J. Numer. Anal. Methods Geomech. 9, 369–381.
Carbone, G., Mangialardi, L., 2004. Adhesion and friction of an elastic half-space in contact with a slightly wavy rigid surface. J. Mech. Phys. Solids 52, 1267–1287.
Chaudhury, M.K., Weaver, T., Hui, C.Y., Kramer, E.J., 1996. Adhesion contact of cylindrical lens and a flat sheet. J. Appl. Phys. 80, 30–37.

Chen, B., Wu, P., Gao, H., 2009. Pre-tension generates strongly reversible adhesion of a spatula pad on substrate. J. R. Soc. Interface 6, 529–537.
Chen, S., Gao, H., 2006a. Non-slipping adhesive contact of an elastic cylinder on stretched substrates. Proc. Roy. Soc. Lond. A 462, 211–228.
Chen, S., Gao, H., 2006b. Non-slipping adhesive contact between mismatched elastic spheres: a model of adhesion mediated deformation sensor. J. Mech. Phys. Solids 54, 1548–1567.
Chen, S., Gao, H., 2006c. Generalized Maugis-Dugdale model of an elastic cylinder in non-slipping adhesive contact with a stretched substrate. Int. J. Mater. Res. 97, 584–593.
Chen, S., Gao, H., 2007a. Bio-inspired mechanics of reversible adhesion: orientation-dependent adhesion for non-slipping adhesive contact with transversely isotropic elastic materials. J. Mech. Phys. Solids 55, 1001–1015.
Chen, S., Gao, H., 2007b. Non-slipping adhesive contact between mismatched elastic cylinders. Int. J. Solids Struct. 44, 1939–1948.
Chen, S., Yan, C., Soh, A., 2009a. Adhesive behavior of two-dimensional power-law graded materials. Int. J. Solids Struct. 46, 3398–3404.
Chen, S., Yan, C., Zhang, P., Gao, H., 2009b. Mechanics of adhesive contact on a power-law graded elastic half-space. J. Mech. Phys. Solids 57, 1437–1448.
Chu, Y.S., Dufour, S., Thiery, J.P., Perez, E., Pincet, F., 2005. Johnson-Kendall-Robert theory applied to living cells. Phys. Rev. Lett. 94, 028102.
De, R., Zemel, A., Safran, S., 2007. Dynamics of cell orientation. Nature Phys. 3, 655–659.
Derjaguin, B.V., Muller, V.M., Toporov, Y.P., 1975. Effect of contact deformations on the adhesion of particles. J. Colloid Interface Sci. 53, 314–326.
Freund, L.B., Lin, Y., 2004. The role of binder mobility in spontaneous adhesive contact and implications for cell adhesion. J. Mech. Phys. Solids 52, 2455–2472.
Fuller, K.N.G., Tabor, D., 1975. The effect of surface roughness on adhesion of elastic solids. Proc. R. Soc. Lond. A 345, 327–342.
Gao, H., Qian, J., Chen, B., 2011. Probing mechanical principles of focal contacts in cell–matrix adhesion with a coupled stochastic–elastic modeling framework. J. R. Soc. Interface 8, 1217–1232.
Gao, H., Wang, X., Yao, H., Gorb, S., Arzt, E., 2005. Mechanics of hierarchical adhesion structures of gecko. Mech. Mater. 37, 275–285.
Greenwood, J.A., 1997. Adhesion of elastic spheres. Proc. R. Soc. London A 453, 1277–1297.
Greenwood, J.A., Johnson, K.L., 1981. The mechanics of adhesion of viscoelastic solids. Philos. Mag. 43, 697–711.
Greenwood, J.A., Johnson, K.L., 1998. An alternative to the Maugis model adhesion between elastic spheres. J. Phys. D: Appl. Phys. 31, 3279–3290.
Giannakopoulos, A.E., Pallot, P., 2000. Two-dimensional contact analysis of elastic graded materials. J. Mech. Phys. Solids 48, 1597–1631.
Giannakopoulos, A.E., Suresh, S., 1997a. Indentation of solids with gradients in elastic properties: Part I. Point force. Int. J. Solids Struct. 34, 2357–2392.
Giannakopoulos, A.E., Suresh, S., 1997b. Indentation of solids with gradients in elastic properties: Part II. Axisymmetric indentors. Int. J. Solids Struct. 34, 2393–2428.
Glassmaker, N.J., Jagota, A., Hui, C.Y., Kim, J., 2004. Design of biomimetic fibrillar interface: 1. Making contact. J. R. Soc. Interface 1, 23–33.
Guduru, P.R., 2007. Detachment of a rigid solid from an elastic wavy surface: theory. J. Mech. Phys. Solids 55, 445–472.
Guo, X., Jin, F., Gao, H., 2011. Mechanics of non-slipping adhesive contact on a power-law graded elastic half-space. Int. J. Solids Struct. 48, 2565–2575.
Haiat, G., Huy, M.C.P., Barthel, E., 2003. The adhesive contact of viscoelastic spheres. J. Mech. Phys. Solids 51, 69–99.
Hui, C.Y., Baney, J.M., Kramer, E.J., 1998. Contact mechanics and adhesion of viscoelastic sphere. Langmuir 14, 6570–6578.
Hui, C.Y., Glassmaker, N.J., Tang, T., Jagota, A., 2004. Design of biomimetic fibrillar interface: 2. Mechanics of enhanced adhesion. J. R. Soc. Interface 1, 35–48.
Hui, C.Y., Lin, Y.Y., Baney, J.M., Kramer, E.J., 2001. The mechanics of contact and adhesion of periodically rough surfaces. J. Polym. Sci., Pt. B, Polym. Phys. 39, 1195–1214.
Hutchinson, J.W., Suo, Z., 1992. Mixed mode cracking in layered materials. Adv. Appl. Mech. 29, 63–191.
Jagota, A., Hui, C.Y., 2011. Adhesion, friction, and compliance of bio-mimetic and bio-inspired structured interfaces. Mater. Sci. Eng. R. 72, 253–292.
Jin, F., Guo, X., 2010. Non-slipping adhesive contact of a rigid cylinder on an elastic power-law graded half-space. Int. J. Solids Struct. 47, 1508–1521.
Johnson, K.L., 1995. The adhesion of two elastic bodies with slightly wave surfaces. Int. J. Solids Struct. 32, 423–430.
Johnson, K.L., Greenwood, J.A., 1997. An adhesion map for the contact of elastic spheres. J. Coll. Interface Sci. 192, 326–333.
Johnson, K.L., Kendall, K., Roberts, A.D., 1971. Surface energy and the contact of elastic solids. Proc. Roy. Soc. Lond. A 324, 301–313.
Kesari, H., Lew, A., 2011. Effective macroscopic adhesive contact behavior induced by small surface roughness. J. Mech. Phys. Solids 59, 2488–2510.
Kim, K.S., McMeeting, R.M., Johnson, K.L., 1998. Adhesion, slip cohesive zone and energy fluxes for elastic spheres in contact. J. Mech. Phys. Solids 46, 243–266.
Long, R., Hui, C.Y., 2012. Axisymmetric membrane in adhesive contact with rigid substrates: analytical solutions under large deformation. Int. J. Solids Struct. 49, 672–683.
Maugis, D., 1992. Adhesion of spheres: the JKR-DMT transition using a Dugdale model. J. Colloid Interface Sci. 150, 243–269.
Persson, B.N.J., 2002. Adhesion between and an elastic body and a randomly rough hard surface. Eur. Phys. J.E 8, 385–401.
Pugno, N., Lepore, E., Toscano, S., Pugno, F., 2011. Normal adhesive force–displacement curves of living Geckos. J. Adhesion 87, 1059–1072.
Popov, G.Ia., 1973a. Plane contact problem for a linearly-deformation foundation in the presence of adhesion. PMM 37, 254–261.
Popov, G.Ia., 1973b. Axisymmetric contact problem for an elastic inhomogeneous half-space in the presence of cohesion. PMM 37, 1109–1116.
Rice, J.R., 1988. Elastic fracture mechanics concepts for interfacial cracks. J. Appl. Mech. 55, 98–103.
Sundaram, N., Farris, T.N., Chandrasekar, S., 2012. JKR adhesion in cylindrical contacts. J. Mech. Phys. Solids 60, 37–54.
Sandukas, S., Yamamoto, A., Rabiei, A., 2011. Osteoblast adhesion to functionally graded hydroxyapatite coatings doped with silver. J. Biomed. Mater. Res. A 97A, 490–497.
Sherge, M., Gorb, S., 2001. Biological Micro- and Nano-Tribology-Nature's Solutions. Springer, Berlin.
Suresh, S., 2001. Graded materials for resistance to contact deformation and damage. Science 292, 2447–2451.
Suresh, S., Mortensen, A., 1998. Fundamentals of Functionally Graded Materials. Institute of Materials, London.
Tsang, P.H., Li, G., Brun, Y.V., Freund, L.B., Tang, J.X., 2006. Adhesion of single bacterial cells in the micronewton range. Proc. Natl. Acad. Sci. 103, 5764–5768.
Walcott, S., Sun, S.X., 2010. A mechanical model of actin stress fiber formation and substrate elasticity sensing in adherent cells. Proc. Natl Acad. Sci. USA 107, 7757–7762.
Waters, J.F., Guduru, P.R., 2010. Mode-mixity-dependent adhesive contact of a sphere on a plane surface. Proc. Roy. Soc. Lond. A 466, 1303–1325.
Waters, J.F., Guduru, P.R., 2011. A mechanism for enhanced static sliding resistance owing to surface waviness. Proc. Roy. Soc. Lond. A 467, 2209–2223.
Waters, J.F., Kalow, J., Gao, H., Guduru, P.R., 2012. Axisymmetric adhesive contact under equibiaxial stretching. J. Adhesion 88, 134–144.
Yao, H., Gao, H., 2006. Mechanics of robust and releasable adhesion in biology: bottom-up designed hierarchical structures of gecko. J. Mech. Phys. Solids 54, 1120–1146.
Yao, H., Gao, H., 2010. Gibson-soil-like materials achieve flaw-tolerant adhesion. J. Comput. Theor. Nanosci. 7, 1–7.